A.J

PCT

INTERNATIONAL APPLICATION PUBLISHED UNDER THE PATENT COOPERATION TREATY (PCT)

(71) Applicant: CALIFORNIA INSTITUTE OF TECHNOLOGY [US/US]; 1201 East California Boulevard, Pasadena, CA 91125 (US).

(72) Inventors: MOSER, Christophe; 965 E. Del Mar #4, Pasadena, CA 91106 (US). BARBASTATHIS, Georgios; California Institute of Technology, Electrical Engineering, 257 Moore, Pasadena, CA 91125 (US). PSALTIS, Demetri; California Institute of Technology, Electrical Engineering, 262A Moore, Pasadena, CA 91125 (US).

(74) Agent: HARRIS, Scott, C.; Fish & Richardson P.C., Suite 1400, 4225 Executive Square, La Jolla, CA 92037 (US).

(54) Title: CONOSCOPIC SYSTEM FOR REAL-TIME CORNEAL TOPOGRAPHY
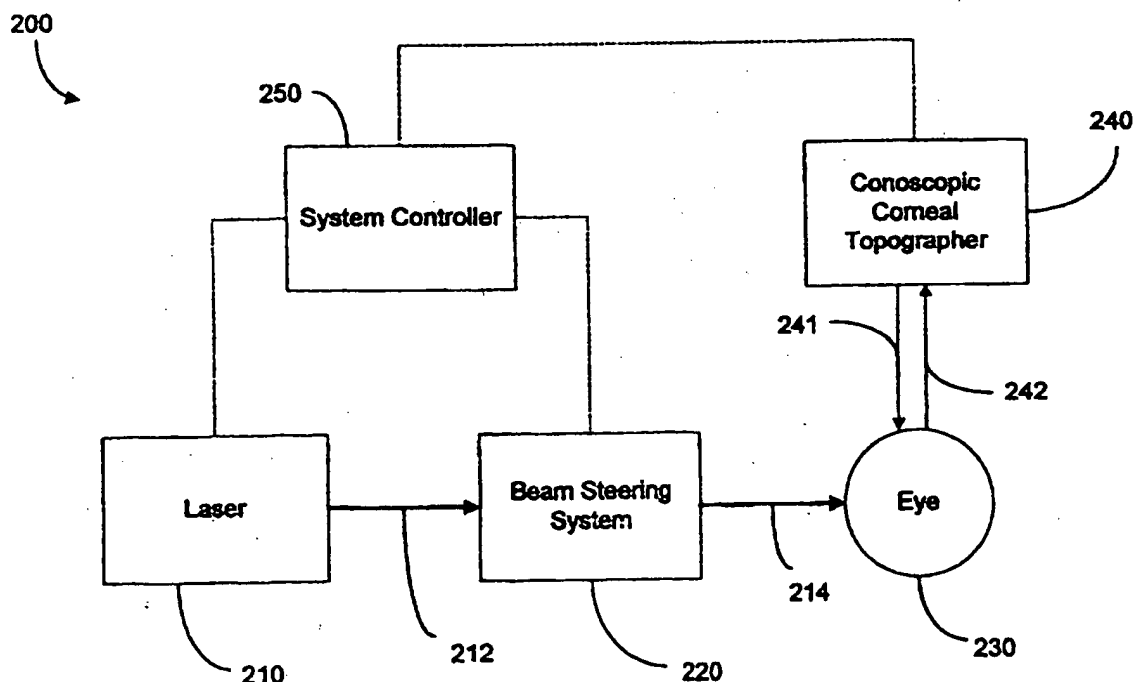
(57) Abstract

   The invention is a corneal topographer (240) based on cornea-scope holography with partially c herent illuminati n. Corneal topographic measurements can be accomplished at a processing rate higher than the standard video rate of 30 Hz. The corneo-scope

CONOSCOPIC SYSTEM FOR REAL-TIME CORNEAL TOPOGRAPHY

CROSS-REFERENCE TO RELATED APPLICATIONS

This application claims the benefits of the U.S.

Provisional Application No. 60/017,539, filed on May 10,

5   1996, and the U.S. Provisional Application No.60/028,945,

filed on October 18, 1996. The disclosure of the above two

provisional applications is incorporated herewith by

reference.

FIELD OF THE INVENTION

10   The invention relates to surface topography using

optical techniques, and more specifically, to a surgical

system for obtaining topographical maps of a cornea based on

optic conoscopic holography.

BACKGROUND OF THE INVENTION

15   Light entering the eye passes through several

refractive elements including the cornea, the aqueous, the

lens, and the vitreous before forming an image on the

retina. Several vision problems are caused by the formation

of defocused images on the retina due to eyeball or corneal

deformations. Some common vision problems include myopia,

5   presbyopia, hyperopia, and astigmatism. Refractive corneal

surgery has been proven to be effective in compensating for

these vision problems by reshaping the cornea, the most

accessible refractive element of the eye, in a way so that

the image focuses correctly on the retina.

10   Corneal shape correction can be achieved with an

invasive surgical procedure such as radial keratectomy,

Kerato-mileusis, and Kerato-phakia. A non-invasive

procedure such as Photorefractive Keratectomy ("PRK") can

also be used in which the corneal surface is ablated

15   step-by-step with ultra-violet (UV) high-power laser pulses

to achieve a desired shape. Another non-invasive procedure

is Laser Photo Thermal Keratoplasty ("LPTK") in which the

cornea is shaped by thermal effects resulting from

irradiation of a laser beam.

The corneal shape determines the corrected vision
acuity. The correction in the corneal curvature is
conventionally measured in diopters, like many other
quasi-spherical optical surfaces. Diopters are defined as a
5   reciprocal of the focal length measured in meters. It is
known that a deviation by 1 diopter from the desired
correction can result in a visual acuity as low as 20/40.
Therefore, accurate measurements of the corneal shape during
the surgical procedure in order to minimize the surgical
10   errors becomes critical.

PRK methods irradiate the patient's eye by a pulsed
laser emitting at a wavelength in an ultra-violet (UV)
spectral region in which the corneal tissue is highly
absorptive. The corneal tissue is ablated by the
15   high-energy laser pulses and the ablation depth produced by
a laser pulse depends on the energy density or "fluence" of
the laser pulse. On average in a typical PRK operation, a
tissue depth of approximately 0.2 ~ 0.4 μm can be ablated
per pulse with a laser fluence ranging from about 100 mJ/cm^2

to about 300 mJ/cm^2.

Two types of PRK procedures are commonly used, one using a uniformly expanded laser beam and another one using a focused scanning beam. The PRK technique based on a uniform beam expand the UV laser beam to approximately the size of the entire cornea. Accurate diameter control may be achieved by using an iris (i.e., a diaphragm). This method can be used in a treatment for the myopia, hyperopia or presbyopia, but not for astigmatism. The scanning beam PRK method focuses the laser beam to a small spot diameter on the cornea (e.g., approximately 1 mm). This small spot diameter is mechanically steered to access different locations on the cornea sequentially. The scanning beam method usually can be used to achieve a desired shaping profile with a better accuracy than that of the uniform beam method.

In many prior-art PRK procedures, a corrective operation is usually done in four steps. First, a desired topographic shape of the cornea of an eye is determined

-4-

based on the specific vision problems in the eye. Secondly,
the operating parameters, such as the total desired ablation
depth and thereby the required number of pulses, are
determined prior to the operation for the desired cornea

5   shape. For a scanning PRK, a desired trace of the scanning
beam also needs to be determined. Thirdly, the
predetermined parameters are used to control the laser to
perform the corrective procedure by reshaping the cornea.
Lastly, the resultant topographical shape of the cornea is

10   measured.

        The above prior-art approach requires that all
predetermined operating parameters remain constant during
operation. For example, the laser fluence must be precisely
known and remain constant during the entire operation. The

15   topographic measurement is performed after the operation and
only then can the success of the operation be evaluated.

        However, a number of practical factors may adversely
affect the above approach. For example, the corneal tissue
may not be even and the absorption coefficient of a cornea

can often have local variations. This may cause variations

in the ablation depth at different locations on the cornea

for a laser beam of a constant fluence. Thus, the final

topographic shape of the cornea may deviate from a desired

5   shape and the resultant vision can be significantly

degraded.

The output power of a laser may also vary or fluctuate

during an operation. This power drift in the laser beam can

be caused by many factors, including temperature variations,

10   mechanical vibrations, noise in the laser electronic control

circuits and so on. In many cases, these factors are not

easily controllable although various control servo

techniques may be used to reduce the variations. The power

variation of the laser can cause undesirable variations in

15   the laser fluence. Consequently, the ablation depth of a

pulse changes.

Furthermore, the alignment of the beam scanning system

is known to change as well due to variations in the relative

positioning of the laser and the beam scanning system,

-6-

variations in the beam scanning system, and beam drift of

the laser. This can cause the scanning laser beam to walk

off from a prespecified scanning trace in a scanning PRK

process, thereby resulting in an error in the final shape of

5   the cornea. Any accidental movement of the eye during the

operation could also adversely affect the operation.

Errors in the final corneal shape due to the above and

other factors significantly reduce the effectiveness of the

PRK procedures. A study of patients who were treated with a

10   conventional PRK at the Doheny Eye Institute of the

University of Southern California showed that about 95% of

the patients achieved a corrected vision acuity 20/40 or

better after the surgery (corresponding to a refractive

error of less than 1 diopter) and only about 50% of these

15   patients had a corrected vision acuity of 20/20 or better.

The current relatively low success probability of PRK at

least in part contributes to the existing doubt of the

public on the PRK procedures despite many benefits and

advantages of the PRK over the use of the corrective eye

glasses or invasive surgical procedures. Many practitioners

in the ophthalmology community believe that a success

probability above 95% in achieving a corrected visual acuity

of 20/20 with PRK may be necessary in convincing more people

5   with visual problems to receive the beneficial PRK

treatment.

In recognition of the above, it is desirable to have

precise active control of the ablation progress in real time

in order to compensate for the above variations during a PRK

10   operation. This requires acquisition of corneal topographic

data of the 3-dimensional shape of the corneal surface

within the time interval between two successive ablating

pulses. In this context, the topographic measurements are

performed in "real time". The topographic data is then fed

15   back to the diaphragm/beam-steering control system to adjust

the operating parameters. This active feedback control

mechanism can be used to minimize the deviation of the final

corneal shape from the ideal shape during the operation.

In order to ascertain the results of the operation,

resolution of 0.1 diopters in the corneal curvature

measurement would be desirable. The amount of diopter

correction as function of ablation depth at the center of

the cornea can be calculated geometrically.

5   The result for the case of myopia is shown in FIG. 1.

The curve in FIG. 1 shows that 0.1 diopters correspond to an

ablation depth of about 1.3 μm which can be achieved with

roughly 4-7 laser pulses in a typical PRK system. At a

pulse repetition rate of 50 Hz, this requires one complete

10   topographical measurement every 80 msec or faster. In a

transverse direction along a corneal surface, the resolution

is mainly determined by the pixel size of the camera and the

apertures of the optics used in the optical system. A

typical camera can provide a resolution of about 250,000

15   pixels. If the entire corneal surface, typically about 29

mm^2 in area, is imaged on the camera, an effective spatial

resolution of approximately 10 μm is obtained. Commercial

systems typically have a resolution on the order of a few

hundred microns. Assuming an acceptable lateral resolution

-9-

at 100 μm in the beam diameter spot, about 2,500 of pixels
need to be processed.

The measured topographic data can be used both for
graphical display and feedback to the beam-steering controls
of the system. To account for delays in the calculation of
the required mirror positions and the mechanical response, a
faster operation of the measurement system may be reasonably
assumed. One estimate for the data processing rate is 30 ms
or 30 Hz, which corresponds to the standard video rate.
This leads to approximately 83,000 pixels per second.

However, the conventional corneal topographic systems
are limited in providing the above real-time topographic
measurements during the surgery. One commercial corneal
topography system, for example, projects calibrated fringe
patterns on the cornea, captures the reflection using a CCD
camera, and then digitally processes the distortions on the
fringe pattern in order to deduce the deviation of corneal
surface from a perfect sphere. The amount of calculation
required to perform this operation cannot be performed at a

speed of 83,000 pixels/sec that is desirable for a real-time.

In addition, the conventional corneal topographic systems impose various other constraints that make them

5   unsuitable for real-time surgical monitoring.

For example, several commercial topographic systems project Placido rings on a corneal surface and capture the specular reflected pattern from the cornea with a camera. The captured pattern is then digitized and measured to

10   determine the fringe distortion. Thus, an one-to-one mapping between the surface deformation and the fringe shape is established. One limitation of this approach is the long processing time, usually on the order of 10 seconds or 0.1 Hz in terms of the processing rate. This is too slow for a

15   real-time corneal topographic measurement required for a PRK treatment. Another limitation is that the Placido ring technique may work well on smooth specularly reflective surfaces but the performance is severely degraded for a scattering or diffusive surface. In a PRK surgery, the

-11-

epithelium on a corneal surface is removed so that the surface is no longer perfectly specular but has a degree of scattering due to the laser ablation. This can undermine the effectiveness of the Placido ring method in a real-time corneal topography during a PRK operation. In addition, the Placido ring method requires the imaging camera to be placed at certain right angles to capture the fringes. This may limit the access of the ablating laser beam to the cornea.

A triangulation technique is also used as a conventional topographic method. A computer controls the pitch of the projected fringes on the corneal surface and acquires the images from the camera. The captured images are processed to obtain the fringe edge distortion data which constructs an isoheight map of the corneal surface. In a binocular configuration, the position of a point of interest on a corneal surface is extracted in three-dimensional space by intersecting the lines connecting the point to two cameras.

One limitation in the binocular-triangulation-based

-12-

technique is the need to have a reference point on the

cornea for a 3D mapping. This is difficult to obtain for a

corneal surface which lacks pronounced features (e.g. a

shape with edges and texture). Another limitation is the

5   requirement to obtain a nearly perfect calibration, since a

slight error in the knowledge about the relative location of

the two cameras can induce large errors in the inferred

surface shape.

Alternatively, a monocular configuration may be used

10 for a triangulation system. Only a single camera is needed.

A light projector can effectively serve as a second, active

camera to replace a second passive camera in the above

binocular configuration. A reference point is no longer

necessary in the monocular technique. The light projector

15 is used to project fringe or grid patterns of varying

spatial frequency on the cornea. The topographic

information is obtained by observing the deformations in the

fringe edges.

Commercial corneal topographers based on triangulation

-13-

can be used for a scattering corneal surface and allow

access to a corneal surface by a ablating laser beam. Since

the camera images a scattering surface at an angle, only a

small portion of the reflected light from the surface may be

5   captured. Therefore, it is often necessary to deposit a

reflectivity enhancing material such as sodium fluorescein

on the cornea in order to improve its reflectivity. The

processing speed is usually slow, typically on an order of 5

to 10 seconds for a full corneal shape on which about 1000

10   points are sampled. In addition, the imaging resolution is

about 0.2 mm.

Coherent holographic interference has also been used in

some commercial topographers. Some aspects of this approach

can be found, for example, in Am. J. Optometry & Phys.

15   Optics, Vol. 65(8), pp. 653-660 (1988) by Smolek and in J.

Cataract Refract. Surg., Vol.19S, pp. 182-187 (1993) by

Burris et al. One limitation of this technique is the

inherent speckle noise in a coherent holographic system.

The inventors of the present invention evaluated this method

-14-

for corneal shape measurements on swine eyes by both

calculations and experiments. It was found that strong

speckle noise was present in the captured images by

illuminating the surface of a swine eye without the

5   epithelium with a laser beam. The speckle noise makes it

very difficult to form a topographic measurement.

Well-known speckle reduction techniques, such as those

disclosed by Iwai and Asakura in "Speckle reduction in

coherent information processing", IEEE proceedings, Vol.

10   84(5), pp.765-781 (1996), are usually cumbersome to

incorporate in a commercial system, and cannot completely

eliminate the speckle noise since they are incompatible with

holographic recording.

The holographic techniques also suffer from power and

15   stability limitations. The allowable power that may be

applied on an eye without causing damage is within a range

approximately from about 300 μW to about 400 μW. A

reflected light beam with about 6-8 μW is usually available

for recording a hologram for a typical eye with a

-15-

reflectivity of about 2%. Conventional photopolymers are

reasonably sensitive media in the red region of the

spectrum. The time required to accumulate enough energy to

record a hologram in such material would be on the order of

5   a few hundred milliseconds, during which the patient's eye

and the optical system must be completely stabilized. This

is difficult in practice because of periodic eye movements

and other instabilities that may occur under surgery room

conditions.

10   **SUMMARY OF THE INVENTION**

In view of the above, the inventors recognized that

conventional corneal topographers are usually not suitable

for monitoring a corneal surface in real time during a PRK

process. The conventional systems are limited by a number

15   of factors including processing speed, noise and geometrical

restrictions.

The present invention as fully disclosed in this

disclosure overcomes these limitations, at least in part, by

-16-

implementing a real-time topographer based on conoscopic

holography. According to an embodiment of the invention, a

partially coherent light source is preferably used to

produce a probe beam for illuminating a target corneal

5   surface of an eye at a fixed position. A collimating

optical element such as a lens collimates the probe beam

which is guided to the target cornea at an angular

incidence. A collecting lens is placed relative to the

target cornea along an optical path of the conoscopic

10   topographer to receive and collimate a reflected probe wave

from the target cornea. A birefringent crystal is

positioned at a predetermined orientation relative to the

collecting lens decomposes the reflected probe wave into

ordinary waves and extraordinary waves. Two mutually-

15   orthogonal polarizers are placed in the optical path with

one on each side of the crystal. An imager such as a CCD

camera is used to capture the conoscopic pattern caused by

the interference between the ordinary and extraordinary

waves. A frame grabber may be used to digitize the

interference pattern. A system controller having a microprocessor is used to extract the three-dimensional topographic information of the reflecting corneal surface.

One aspect of the present invention is the use of conoscopic holography to capture the topographic information of a corneal surface. One advantage of this approach is a high resolution which is on an order of one wavelength. Another advantage is a single-step detection of deformation in the corneal surface. Yet another advantage is the use of partially coherent or incoherent light sources to minimize the speckle noise caused by a specular reflection from the cornea.

Another aspect of the invention is a hybrid opto-electronic system for the extraction of a corneal shape. The corneal shape is optically imprinted on the wavefront of the reflected probe beam and is recorded in conoscopic interference fringes. The corneal shape is then extracted by capturing the optical conoscopic interference pattern with an imager and processing the topographic

-18-

information with a microprocessor. According to one

embodiment, the microprocessor is programmed to perform a

corneal shape extraction from the sheared interferogram

based on a technique using Hermite polynomial expansions.

5   This aspect of the invention allows a high speed operation

and provides a real-time measurement in PRK operations.

        Yet another aspect is a measurement of the deviation of

a corneal surface from a desired model shape based on the

conoscopic interference pattern. A conoscopic topographer

10   in accordance with the invention can be implemented in a PRK

system to improve the performance of PRK operations with

high accuracy and minimal human intervention. In

particular, the corneal surface can be measured in real time

between ablating laser pulses to monitor ablation result of

15   each pulse. The measurements can be fed back in a servo

control to adjust the driving mechanism of the ablating

laser and the beam control system, thus allowing a accurate

control of the ablation profile.

-19-

BRIEF DESCRIPTION OF THE DRAWINGS

These and other aspects and advantages of the present

invention will become more apparent in light of the

following detailed description of preferred embodiments

5   thereof, as illustrated in the accompanying drawing, in

which:

FIG. 1 is a chart showing ablation depth at the center

of the cornea as a function of achieved diopter correction

. for myopia.

10   FIG. 2 is a block diagram of a preferred embodiment of

a PRK system with a conoscopic topographer.

FIG. 3 is a schematic illustration of a tilted crystal

geometry for conoscopic holography.

FIG. 4 is a photograph of a typical conoscopic pattern

15   obtained with the system of FIG. 3.

FIG. 5 is a schematic diagram of a special

configuration of a conoscopic topographer in accordance with

the invention.

FIG. 6A is a schematic diagram showing a conoscopic

geometry for extracting a corneal shape.

FIG. 6B is a simplified conoscopic geometry that is equivalent to the geometry of FIG. 6A.

FIG. 7 is a flowchart of a shape extraction method based on conoscopic holography in accordance with the invention.

5

DETAILED DESCRIPTION OF THE PREFERRED EMBODIMENT

FIG. 2 is a block diagram showing one embodiment 200 of

the PRK surgical system with a conoscopic corneal

topographer 240 of the invention. The dashed lines indicate

electrical signals and the arrowed lines indicated optical

signals. A laser 210 is preferably a UV laser operating in

a spectral range in which the corneal tissue is absorptive.

Excimer lasers emitting at wavelengths from about 150 nm to

250 nm are widely used for PRK. Other lasers may also be

used, such as UV solid-state lasers and diode-pumped lasers.

A beam 212 produced by the laser 210 is guided to a target

eye 230 as a beam 214 by a beam steering system 220. The

laser 210 preferably produces a pulsed laser output. The

pulse repetition rate and the pulse duration of the laser

210 may be adjusted.

The beam steering system 220 may have at least one

mirror mounted on a galvanometer or other motion control

device. The beam steering system 220 may have beam

focusing optics for performing a scanning beam PRK operation

-22-

or a beam expander for performing a uniform beam PRK

operation. Therefore, the beam 212 and the beam 214 may

have different beam properties, for example, different beam

diameters and divergence.

5   A system controller 250 may include a microcontroller

or a microprocessor for controlling the operations of the

PRK system 200. For example, the output energy or power of

the laser 210 may be controlled at any time by the system

controller 250 to change the laser fluence at the surgical

10   spot on the eye 230. Alternatively, the laser output may be

changed by an electrically-controlled beam attenuator

deployed in the path of the laser beam. The system

controller 250 also controls the operation of the beam

steering system 220 to guide beam 214 to a desired location

15   on the target eye 230. A user may program the system

controller 250 so that the focused beam 214 is scanned on

the corneal surface of the eye 230 over a predetermined

trace pattern in a scanning beam PRK operation.

A conoscopic corneal topographer 240 in the PRK system

-23-

200 is a corneal topographer based on the conoscopic

holographic technique. A probe beam 241 is generated by an

independent light source in the topographer 240. The probe

beam 241 illuminates the cornea to produce a reflected probe

5   beam 242 which is indicative of the phase variations of the

cornea surface. A birefringent optical medium is deployed

in the topographer 240 to generate a conoscopic interference

pattern by the interference between an ordinary wave and an

extraordinary wave of the reflected beam 242. The

10   interference pattern represents the phase information of the

corneal surface which is indicative of the topographical

shape of the cornea. The interference pattern is then

processed by the system controller 250 to extract the

topographic shape of the cornea. The topographic shape of

15   the cornea obtained from the topographer 240 provides an

accurate measurement of the corneal surface ablated by the

ablating laser beam 214.

The topographer 240 in accordance with an embodiment of

the invention can process the corneal topographic

information during the PRK operation at a processing rate

higher than the pulse repetition rate of the laser 210.

Thus, the topographic measurement can be used to monitor the

results from each pulse of the ablating laser beam 214.

5   This allows detection of the desired ablation depth at a

desired location on a pulse by pulse basis.

An ideal topographic shape of the cornea of a patient's

eye is predetermined based on a diagnosis of the patient's

eye condition and the desired corrected vision that is to be

10   achieved by the PRK treatment. The topographic information

of the ideal cornea shape is stored in a memory unit of the

system controller 250.

According to the present invention, the real-time

topographic measurements can be used to control the laser

15   210 or the beam steering system 220. Any deviation from the

predetermined ideal topographic shape may be corrected in

real time during the PRK operation. As described above, the

laser fluence may vary or fluctuate and the ablating beam

position on the cornea may "walk off" from the desired beam

-25-

trace. In addition, the surface properties of a cornea may

not be uniform across the entire corneal surface. In

particular, the absorption coefficient of the cornea may

have local variations. These and other factors can

5   adversely affect the outcome of a PRK operation. By

dynamically adjusting the ablating laser beam position and

the laser fluence based on the ablation depth and ablated

location of a precedent laser pulse, the system 200 can

significantly improve the performance of the PRK operation

10   over the conventional systems.

For example, the system controller 250 may command the

beam steering system 220 to adjust the beam positioning on

the corneal surface of the ablating beam 214 based on the

topographic measurement directly after a preceding pulse.

15   This may show that the preceding pulse is deviated from a

desired ablating trace. If topographic measurement right

after a preceding pulse indicates that the ablation depth

produced by a preceding laser pulse has deviated from the

ideal depth due to a variation in the laser fluence or in

the absorption coefficient of the cornea in that region, the

system controller 250 may control the laser 210 to adjust

the laser fluence of a subsequent laser pulse to a corrected

value.

5   A preferred embodiment for the conoscopic corneal

topographer 240 is based on the concept of conoscopic

holography.   See, for example, Sirat and Psaltis in

"Conoscopic Holography", Optics Letters, Vol. 10(1), pp. 4-6

(1985), Sirat in "Conoscopic Holography. I. Basic principles

10   and physical basis", Journal of Optical Society of America,

Vol. A9(1), pp. 70-83 (1992) and "Conoscopic Holography. II.

Rigorous derivation", Journal of Optical Society of America,

Vol. A9(1), pp. 84-90 (1992).   Conoscopic holography is a

method for forming interference fringes with quasi-

15   monochromatic but not necessarily coherent light sources.

It is implemented with a highly birefringent optical medium,

for example, a calcite crystal.   The birefringent crystal is

illuminated by a linearly-polarized light from a light

source.   Each ray entering the crystal is refracted into two

-27-

types of rays, an ordinary ray ("o-ray") and an

extraordinary ray ("e-ray"). These two types of rays

experience different phase delays because of their different

indices of refraction in the crystal, unless both rays

5   propagate along a crystal optic axis. An interference

pattern can be obtained by the interference between the two

different rays.

FIG. 3 shows a special conoscopic holography

configuration 300 with a tilted uniaxial birefringent

10   crystal in accordance with the present invention. The

system 300 includes a quasi-monochromatic point source 310,

a lens 340, a birefringent crystal 350, and a polarizer 360

that are positioned relative to one another to form an

optical train along a system optic axis 312. The point

15   source 310, which can be coherent, partially coherent, or

incoherent, is located at or close to the front focal plane

342 of the lens 340. The crystal 350 has a crystal optic

axis 352 along which an o-ray and an e-ray undergo the same

phase delay. The crystal 350 is disposed in an orientation

-28-

to form a tilted angle 351 (Ψ) with the system optic axis

312.   Two exemplary light rays 320 and 330 from the point

source 310 are shown in FIG. 3 to illustrate the operation.

The rays 320 and 330 divide into their own o-rays, 324 and

5   334, and e-rays, 322 and 324, respectively, since rays 320

and 330 do not propagate along the crystal optic axis 352

due to the tilting of the crystal.

The o-ray 324 coming from the ray 320 can combine with

the e-ray 332 from the ray 330 at the exit surface 356 for a

10   proper spatial separation of rays 320 and 330 on the

entrance face 354 of the crystal 340.   The two modes are

mixed by using the polarizer 360 to form an interference

pattern due to the difference in phase delay between the two

interfering rays 324 and 332.   The conoscopic interference

15   pattern of a simple point source is similar to a Fresnel

zone plate with a superimposed cross (bright or dark,

depending on the analyzer orientation) parallel to the

eigenaxes.   The cross may be eliminated using circularly

polarized light.   FIG. 4 shows a typical conoscopic pattern

-29-

obtained with a tilted calcite crystal in the system 300.

It is known that the interfering rays in a conoscopic setup typically sustain very small path difference and they originate at neighboring locations if an extended source is

5   used. Therefore the temporal and spatial coherence requirements for a high-contrast interference pattern are much less stringent than the conventional coherent holographic interferometric techniques. As a result, only near-monochromaticity is required for the light source in a

10   conoscopic setup. Thus, a variety of light sources may be used for conoscopic holography, including a light source that is both temporally and spatially coherent (e.g., a laser) and a highly incoherent quasi-monochromatic light source (e.g., a gas discharge lamp). The point source 310

15   is used here for simplification of the geometry.

The interference intensity pattern is a function of the total phase difference between the interfering beams from the point source 310 to the interfering point (e.g., 358) on the exit surface 356 of the crystal 350. Specifically, the

fringe spacing is related to the defocus distance Δf between the point source 310 and the focal plane 342, the focal length f of the lens 340, the tilt angle 351 (Ψ), the thickness L, and the refractive properties of the uniaxial crystal 356.

Let $G(x)$ be the total optical path difference and x be the radial distance from the system optic axis 312 to the interfering point 358. The optical intensity of the interference pattern after the polarizer 360 can be approximately expressed as:

$$I(x) = \frac{I_0}{2}\left[1 + \cos\left(\frac{2\pi G(x)}{\lambda}\right)\right] \qquad (1)$$

where I_o is an averaged light intensity in the interference field received by the imager. The optical path difference, $G(x)$, can be calculated for the specific geometry of the conoscopic configuration. For the conoscopic system 300

-31-

using the uniaxial birefringent crystal 350 with indices of refraction for the ordinary and extraordinary rays as n_o and n_e, $G(x)$ can be shown to have the following form:

$$G(x) = n_0 L \left(\frac{n_e}{\sqrt{n_e^2 - \sin^2(\Psi - \theta_e(x))}} - \frac{n_o}{\sqrt{n_o^2 - \sin^2(\Psi - \theta_o(x))}} \right) +$$

$$L \left(\frac{n_o}{n_e} \frac{\sin(\Psi - \theta_e(x))}{\sqrt{n_e^2 - \sin^2(\Psi - \theta_e(x))}} - \frac{\sin^2(\Psi - \theta_o(x))}{\sqrt{n_o^2 - \sin^2(\Psi - \theta_o(x))}} \right) \times$$

$$\left\{ \sin\Psi + \frac{\Delta f \cos^2 \Psi}{2 f (f + \Delta f)} \left[L \left(\frac{n_o}{n_e} \frac{\sin(\Psi - \theta_e(x))}{\sqrt{n_e^2 - \sin^2(\Psi - \theta_e(x))}} + \right. \right. $$

$$\left. \left. \frac{\sin^2(\Psi - \theta_o(x))}{\sqrt{n_o^2 - \sin^2(\Psi - \theta_o(x))}} \right) - 2x \right] \right\}, \qquad (2)$$

where θ_o and θ_e are given by:

$$\theta_o(x) = \frac{\left(x - L\dfrac{\sin(\Psi - \theta_o(x))}{\sqrt{n_o^2 - \sin^2(\Psi - \theta_o(x))}}\right)\cos\Psi}{f\left(1 + \dfrac{f}{\Delta f}\right) - a - \left(x - L\dfrac{\sin(\Psi - \theta_o(x))}{\sqrt{n_o^2 - \sin^2(\Psi - \theta_o(x))}}\right)\sin\Psi}, \qquad (3)$$

$$\theta_e(x) = \frac{\left(x - \dfrac{n_o}{n_e}L\dfrac{\sin(\Psi - \theta_e(x))}{\sqrt{n_e^2 - \sin^2(\Psi - \theta_e(x))}}\right)\cos\Psi}{f\left(1 + \dfrac{f}{\Delta f}\right) - a - \left(x - \dfrac{n_o}{n_e}L\dfrac{\sin(\Psi - \theta_e(x))}{\sqrt{n_e^2 - \sin^2(\Psi - \theta_e(x))}}\right)\sin\Psi}. \qquad (4)$$

The distance a in Eqs. (3) and (4) is the distance from the lens 340 to the intercept point 353 of the system optic axis 312 and the entrance surface 354 of the crystal 350. A set of similar equations can be derived for the y-direction since the optic axis of crystal is in the xz-plane. The description of the y-direction will be neglected throughout the disclosure for simplicity.

FIG. 5 is a schematic illustration of a special

-33-

implementation of the real-time conoscopic corneal

topographer 240 of the PRK system 200 (FIG. 2) based on the

conoscopic system 300 of FIG. 3. The conoscopic

interference pattern is generated by a reflected probe beam

5   off an eyeball.

A partially coherent light source 410 is preferably

used to illuminate the eyeball 240 at a fixed position.

Collimating optics 520 (e.g., a lens) collimates a light

beam 512 produced by the light source 510. The collimated

10   beam 514 is then directed to pass through an iris 540 to

illuminate the eyeball 240. At least one mirror 530 may be

optionally used to facilitate the guidance of the collimated

beam 514. Preferably, the collimated beam 514 is incident

to the eyeball 240 at an angle as illustrated in FIG. 5

15   because the ablating laser beam 214 produced by the laser

210 needs to impinge the eyeball 240 at a near normal

incidence. The angular incident geometry of the probe beam

allows easy access to the cornea by the ablating laser beam

240 and does not adversely affect the performance of the

topographer.

A portion of the collimated beam 514 is reflected by
the eyeball 240 as a reflected beam 516. Since the eyeball
240 has an approximately spherical shape, the reflected beam
5   516 diverges. A collecting lens 550 is placed relative to
the eyeball 240 along the optical path of the conoscopic
topographer approximately re-collimates the light beam 516
and directs the reflected beam to the birefringent crystal
350 that is sandwiched between two crossed polarizers, a
10   polarizer 560 and an analyzer 570. An imager 580, such as a
CCD camera, is positioned behind the polarizer 570 to
capture the conoscopic interference pattern imprinted in the
light beam emerging from the birefringent crystal 350. A
frame grabber 582 may be used to digitize the interference
15   pattern. The interference pattern is then fed to the system
controller 250 and is processed to extract the information
about the curvature and shape of the reflecting corneal
surface.

An alignment laser (not shown) is often used to

-35-

facilitate fixing the target eye 240. The alignment laser

is usually a low-intensity red laser that produces a red

beam in the direction of the ablated beam 214. A patient

lies down on a table and is asked to look at the red beam.

5   This aligns the red beam to be substantially perpendicular

to the target eye 240. Therefore, the ablating beam 214 is

also substantially perpendicular to the target eye 240.

One way to align the collecting lens 550 is by using

the interference fringes after the analyzer 570. The

10   collecting lens 550 may be mounted on a positioner to

facilitate the alignment. A suitable positioner can be, for

example, a translation stage or a piezo device for precise

positioning control. The collecting lens 550 is adjusted to

a position relative to the eye 240 at which the spacing of

15   the observed conoscopic fringes is maximized.

The polarizer 560 is preferably placed between the eye

240 and the crystal 350. However, the polarizer 560 may be

placed anywhere in the optical path of the probe beam prior

to entering the crystal 350. According to the present

-36-

invention, the reflected probe beam at the entrance surface

of the crystal preferably has such a linear polarization

with respect to the orientation of the crystal so that the

ordinary and extraordinary waves have a substantially equal

5   intensity relative to each other. This desired condition

increases the contrast of the interference pattern.

For a Cartesian coordinate system in the special system

500 of FIG. 5, the polarizer 560 preferably has an angle of

45° with respect to either the positive x direction or the

10   negative x direction.

The special system 500 is preferably calibrated by

using a reflective spherical surface with known dimensions.

A metallic calibration sphere may be used, for example.

Since the exact shape of the calibration sphere is known,

15   the optical aberration errors of the system 500 can be

measured by the actual shape measurements with the

calibration sphere. This calibration results are stored in

the system controller 250 for calibrating measurements.

The inventors discovered that the coherence properties

-37-

of the light source 510 can significantly affect the

performance of the real-time conoscopic topographic

measurements. The light source 510 should be selected based

on the performance specifications of the system and the

5   requirements of the conoscopic interferometry. The

following factors are used in selecting a proper light

source 510:

1.   The spatial coherence of the light source 510

is necessary for achieving a good visibility or

10   contrast of the conoscopic fringes. The

visibility improves as the degree of spatial

coherence of the light source 510 increases.

2.   The noise performance of the conoscopic

system deteriorates as the degree of temporal

15   coherence of the light source 510 increases due to

the speckle noise caused by the interference of

rays reflected from neighboring points on a

specular surface.

3.   The wavelength and the power level of the

light source 510 should be eye-safe. An eye-safe

power level is considered at about 200μW. The

wavelength for the probe beam produced 510 may be

from the visible spectrum to the IR range.

5   4.   Since the reflectivity of the eye is

typically about only 2%, the light source 510

should be sufficiently strong within the eye-safe

power limit in order to achieve a sufficient

signal intensity at the imager 580. The laser

10   power delivered to the entire cornea is preferably

at approximately 100μW or more if a typical

commercial CCD array is used as the imager 580.

The laser power at the cornea may vary depending

on the detection efficiency and sensitivity of the

15   imager 580 used.

The inventors tested the special system 500 with

various light sources based on the above guidelines. In

testing the system 500, a uniaxial calcite crystal of 30mm x

30mm x 40mm was used as the birefringent crystal 350, a CCD

-39-

camera manufactured by the ImagePoint Corporation was used

as the imager 580, and a Pentium personal computer was used

as part of the system controller 250. The tests were

performed with swine eyes *in vitro*. Test results with four

5   types of light sources, lasers, current-swept laser diodes,

sodium lamps, and VCSELs are summarized in Table 1.

TABLE 1

Source	Advantages	Problems
HeNe laser	high power high spatial coherence	strong speckle potential dangerous
Sodium lamp	no speckle	low power low fringe visibility (low spatial coherence)
Laser diode, current-swept	power & coherence	strong speckle (insufficient sweeping range)
VCSEL, small bandwidth (Linewidth< 7×10^{-3} nm)	power & coherence	strong speckle
Super Luminescent diode linewidth ~10 nm	no speckle sufficient power	medium fringe visibility (limited spatial coherence)

The tests clearly show the trade-off between the

coherence of the light source and the noise performance of

the conoscopic topographer. Light sources with high spatial

-40-

and temporal coherence such as a He-Ne laser and a

vertical-cavity surface-emitting laser diode ("VCSEL") with

a narrow bandwidth (e.g., less than 7 x 10^{-3} nm) can produce

fringes with high visibility in imaging optical quality

surfaces. However, these highly coherent light sources

produce strong speckle noise when used with highly specular

surfaces such as the corneal surface. On the other hand,

incoherent sources such as a sodium lamp can yield low power

efficiency because of a wide angular emission distribution

and poor fringe visibility. Since spatial coherence is

necessary, a pin hole may be placed in front of an

incoherent light source (e.g., sodium lamp) to increase the

degree of the spatial coherence of the probe beam impinging

on the cornea. The use of the pin hole significantly

reduces the useful probe beam power. The speckle noise,

however, is greatly reduced compared to the results of

coherent light sources.

The best results were obtained using a super

luminescent diode (e.g., Hamamatsu L3302) among the tested

-41-

light sources listed in Table 1. The super luminescent

diode operates at λ = 850 nm with a bandwidth about 10nm.

This offers a balance between the coherence and speckle

noise. A VCSEL made by Honeywell can also be used, which

5   has a nominal bandwidth of about 0.5 nm near 850 nm. A

degree of monochromaticity of the light source 510 can be

characterized by a ratio of the emission linewidth $\Delta\lambda$ and

the center wavelength λ. According to the invention, $\Delta\lambda/\lambda$

is preferably in a range from about 0.1% to about 1% for

10   typical corneal measurements. This range may change

depending on the requirements of a specific application.

FIG. 6A illustrates an actual geometry 600 for

extracting the three-dimensional corneal surface shape based

on the conoscopic system 500. A collimated light beam 610

15   is incident upon the corneal surface of an eye 240 at an

angle. The beam 610 is reflected to pass through a lens

340, a tilted uniaxial birefringent crystal 350, and a

polarizer 360. Assume that the o-ray 622 of a ray 620 and

the e-ray 632 of a ray 630 within the crystal 350 interfere

with each other at a point 358 on the exit surface 356 and
the rays 620 and 630 respectively originate at points 621
(ξ_o) and 631 (ξ_e) on the corneal surface of the eye 240.
According to the present invention, the system controller

5   250 can be programmed to extract the corneal surface shape
by processing the digitized fringe pattern based on the
specific geometry of the conoscopic system.

FIG. 6B shows a different geometry 601 that is
equivalent to the actual geometry 600 in extracting the

10   corneal shape. The equivalent geometry 601 is similar to
the conoscopic geometry 300 of FIG. 3 with an addition of a
transmissive phase aberrator 640. There are several
differences between the actual geometry 600 and the
equivalent geometry 601. In the actual geometry 600 for the

15   corneal topography, the corneal surface to be measured is
reflective rather than transmissive; the corneal surface is
quasi-spherical rather than planar; the light is incident to
the corneal surface at an angle rather than a normal
incidence. However, there is an one-to-one correspondence

-43-

between the systems 600 and 601 of FIGs. 6A and 6B, which is

defined by a set of geometrical transformations. The

geometry 601 is used to simplify the mathematical complexity

of the extracting algorithm without losing physical traits

5   of the actual geometry 600. For example, the phase

distortion caused by the phase aberrator 640 is equivalent

to the phase distortion of the corneal surface of the system

240 in the actual geometry 600. Therefore, it suffices to

restrict the description of the extraction of the corneal

10   shape to the simplified geometry 601 of FIG. 6B.

Referring to FIG. 6B, each ray emanating from the point

source 310 attains a different phase-shift $\phi(\xi)$ depending on

the point of intersection ξ with the phase aberrator 640.

The rays emitted by the point source 310 are collected by

15   the lens 340 of a focal length f after passing through the

phase aberrator 640. The point source 310 is located a

distance, $(f+\Delta f)$, away from the lens 340, therefore the

light beam past the lens 340 has a degree of sphericity

depending on the defocus Δf. As explained above, an

-44-

interference pattern forms behind the polarizer 360 due to

the phase difference between the e- and o-rays converging to

the point 358 at the exit face 356 of the crystal 350. The

two rays 620 and 630 intersect the aberrator surface at ξ_e

5   and ξ_o respectively, which correspond to the two points 621

and 631 on the corneal surface of the eye 240 in FIG. 6A.

The conoscopic interference pattern I(x) obtained after

the polarizer 360 can be approximately expressed in the

following form:

$$I(x) = \frac{I_o}{2}\left[1 + \cos\left(\frac{2\pi G(x)}{\lambda}\right) + \phi(\xi_e) - \phi(\xi_o)\right], \qquad (5)$$

10   where G(x) is given by Eq. (1). The extraction can be

accomplished with the following three steps as shown in a

flowchart 700 in FIG. 6.

In step 1 at 710, the phase difference $\phi(\xi_e) - \phi(\xi_o)$ is

-45-

extracted by using a phase shifting method. Referring to

FIG. 6B, the orientation of the birefringent crystal 350

about the y axis is changed to alter the optical path

difference G(x) and thereby induces a phase shift in the

5   interference pattern. Four different tilting angles of the

crystal 350 are chosen in the following manner. An

interference pattern I(0) is measured at an initial

orientation of the crystal 350 at a tilt angle Ψ_0. The tilt

angle Ψ is then increased from Ψ_0 to a value Ψ_1 such that

10   the phase shift in the interference pattern with respect to

the initial title angle Ψ_0 is $\pi/2$. The measured

interference pattern at Ψ_1 is represented by $I(\pi/2)$. The

tilt angle Ψ is subsequently increased to Ψ_2 and Ψ_3 to

obtain interference patterns $I(\pi)$ and $I(3\pi/2)$, respectively.

15   All measurements are performed for the same corneal surface.

Based on the phase-shifted intensity patterns, the phase

difference in Eq. (5) can be evaluated according the

following equation:

$$\phi(\xi_e) - \phi(\xi_o) = atan\left(\frac{I(\frac{3\pi}{2}) - I(\frac{\pi}{2})}{I(0) - I(\pi)}\right). \tag{6}$$

The phase difference $\phi(\eta_e) - \phi(\eta_o)$ in an orthogonal direction (η) with respect to ξ can be obtained in a similar manner.

The above phase shifting technique also allows a determination of the averaged intensity I_0 in Eq. (5). The intensity I_0 may be subtracted from the detected intensity pattern.

In step 2 at 720, a transformation between the coordinate x in the interference pattern captured by the imager 580 and the coordinates ξ_e and ξ_o on the phase aberrator 640 (equivalently, the coordinates in the x direction on the cornea) is performed. Thus, the positioning of the 2D interference pattern is transformed into 2D coordinates of the corneal surface in the xy-plane. A geometrical calculation shows that this relationship can be expressed with a quadratic formula, which may be stored

-47-

in a look-up table. In a particular case where there is no

defocus ($\Delta f = 0$), the following linear approximation may be

used for the transformation for small crystal tilt angle Ψ:

$$\frac{\xi_e + \xi_o}{2} = 2x - (\gamma_e + \gamma_o) L,$$

(7)

where γ_e and γ_o are given by the following equations:

$$\gamma_e = \frac{\sin\Psi}{\sqrt{n_e^2 - \sin^2\Psi}},$$

(8)

$$\gamma_o = \frac{\sin\Psi}{\sqrt{n_o^2 - \sin^2\Psi}}.$$

(9)

5   In step 3 at 730, the spatial gradient of the phase

difference, $\Delta\phi(\xi_e) - \Delta\phi(\xi_o)$, on the corneal surface is

determined. The corneal surface variation along the z-

-48-

direction can be determined. Therefore, the results of the

steps 2 and 3 can be combined to extract three-dimensional

surface shape. This is shown by a step 740 in FIG. 6.

According to the present invention, a preferred

5   extraction technique uses a set of polynomials to represent

the phase information of the corneal surface. For

illustration purpose, mutually-orthogonal Hermite

polynomials are used below as an example to the polynomial

technique although other polynomials may also be used. Only

10   one-dimensional analysis is described.

Hermite polynomials are conventionally defined as

follows:

$$H_n(x) = (-1)^n e^{x^2} \frac{d^n}{dx^n} e^{x^2}.$$ (10)

It is known that any real function $\phi(x)$ with countable

discontinuities can be uniquely expanded in terms of Hermite

15   polynomials as follows:

-49-

$$\phi(x) = \sum_{j=0}^{\infty} b_j H_j(x).\tag{11}$$

In a typical practical application, the upper limit of the

summation in Eq. (9) can be restricted to a selected finite

integer J to achieve a sufficient accuracy. The specific

number J is determined based on the requirements of an

5   application and may vary from one application to another.

If the function $\phi(x)$ contains components $j>J$, then integer J

represents the accuracy of the polynomial expansion.

Specifically, an upper summation limit of $J=6$ may be

sufficient in many practical cases to obtain relatively

10   smooth functions for mildly-deformed spherical surfaces such

as the human cornea. Therefore, for a prespecified integer

J, Eq. (9) can be approximated as:

$$\phi(x) = \sum_{j=0}^{J} b_j H_j(x).\tag{12}$$

The extraction of the corneal shape involves a
difference function $\omega(x)$ of two functions of the same
mathematical form with different variables as indicated by
Eq. (5). The difference function $\omega(x)$ is recorded by the
5   imager and is known. In term of the Hermite polynomials,
$\omega(x)$ can be written as:

$$\omega(x) = \phi(x+h) - \phi(x)$$
$$= \sum_{j=0}^{J} b_j [H_j(x+h) - H_j(x)], \tag{13}$$

where h represents the spatial separation of the ordinary
and extraordinary rays at the exit surface 356 of the
crystal 350 caused by the birefringence and b_j are the
10   expansion coefficients which are to be determined. If the
expansion coefficients b_j are known, the spatial gradient of

-51-

the phase difference corresponding to the phase variation on the corneal surface is known. The surface shape can then be determined.

Alternatively, the difference function $\omega(x)$ may be approximately expressed in another expansion of the Hermite polynomials with a different set of coefficients c_j up to $(J-1)$ order:

$$\omega(x) = \phi(x+h) - \phi(x) \approx \sum_{j=0}^{J-1} c_j H_j(x).$$

(14)

Since $\omega(x)$ is known by measurements, the expansion coefficients c_j can be readily derived by projecting $\omega(x)$ in the vector space $H_j(x)$ based on Eq. (12).

The shifted Hermite polynomials are known to have the following property:

-52-

$$H_n(x+h) - H_n(x) = \sum_{k=0}^{n-1} \frac{n!}{k!\,(n-k)!} (2h)^{n-k} H_j(x). \tag{15}$$

Using the above relation, the expansion coefficients, b_j, can be determined by using c_j. This is shown in the following Eqs. (14) and (15):

$$b_j = \frac{c_{j-1}}{2jh}, \tag{16}$$

$$b_j = \frac{1}{2jh} \left[c_{j-1} - \sum_{k=j+1}^{J} \frac{k!}{(j-1)!\,(k-j+1)!} (2h)^{k-j+1} b_k \right]. \tag{17}$$

The coefficient b_j is first determined by Eq. (14).

Other b_j can be subsequently determined with c_j and b_J by applying Eq. (15) for j decreasing from J down to 1. Each step requires only the coefficients calculated from the previous steps. Hence, the computational complexity is $O(J)$. Note also that the coefficient b_0 is not included in Eqs. (14) and (15). This does not affect the measurement because b_0 is simply a constant bias and can be ignored.

One advantage of the Hermite polynomial expansion is that the difference pattern can be expressed analytically as shown by Eq. (13). This process is computationally simple and can be completed in a short computing cycle. This reduces computational cost. Another advantage is that it does not have singularity problems, which further simplifies the processing process.

Although the present invention has been described in detail with reference to a preferred embodiment, one ordinarily skilled in the art to which this invention pertains will appreciate that various modifications and enhancements may be predictable.

-54-

For example, the conoscopic topographer in accordance
with the invention may be used for corneal shape
measurements unrelated to PRK, such as the evaluation of
radial keratectomy or thermo-laser keratoplasty. One of the
advantages of using the conoscopic topographer is the better
accuracy compared to conventional corneal topographers. The
accuracy of a topographer according to the invention is on
an order of one wavelength based on the fringe measurements.
Other reflective surfaces that are substantially spherical
may also be measured.

The spatial gradient of the phase difference between
the ordinary and extraordinary waves may also be determined
with other methods in addition to the Hermite polynomial
technique. One alternative method calculates the spatial
gradient at mid-points $\xi \approx (\xi_e + \xi_o)/2$, $\eta = (\eta_e + \eta_o)/2$ by the
following approximation:

$$\frac{\partial \phi(\xi, \eta)}{\partial \xi} \approx \frac{\phi(\xi_e) - \phi(\xi_o)}{\xi_e - \xi_o}, \qquad (18)$$

-55-

$$\frac{\partial \phi(\xi, \eta)}{\partial \eta} = \frac{\phi(\eta_e) - \phi(\eta_o)}{\eta_e - \eta_o}. \qquad (19)$$

The actual height variation map of the corneal surface is extracted by a Taylor expansion approximation. The accuracy of this method is limited, especially at a location where the corneal surface has a steep variation in shape.

Another alternative method is based on fast Fourier transform ("FFT") of the conoscopic interference pattern. Assume $\Phi(u, v)$ is the Fourier transform of the unknown height map:

$$\Phi(u, v) = F[\phi(\xi, \eta)]. \qquad (20)$$

The phase difference can be transformed as the following:

-56-

$$G_\xi(u,v) \equiv F[\phi(\xi,\eta) - [\phi(\xi+h_\xi,\eta)]$$

$$= (1-e^{i2\pi uh_\xi})\Phi(u,v), \qquad (21)$$

$$G_\eta(u,v) \equiv F[\phi(\xi,\eta) - [\phi(\xi,\eta+h_\eta)]$$

$$= (1-e^{i2\pi vh_\eta})\Phi(u,v). \qquad (22)$$

By inverting the above Fourier transforms, the original

surface $\phi(\xi,\eta)$ is reconstructed with ambiguity only at

spatial frequencies equal to multiples of $1/h_\xi$, $1/h_\eta$, that

is, at the singularities of the shear kernel. Since mainly

point-to-point operations or fast-Fourier transforms are

involved in the FFT method, the operation may be performed

at a high speed with dedicated electronics in the system

controller 250. Allowing 20 msec for the phase extraction

in the step 1 which is the most computationally expensive,

-57-

the remaining two steps can be performed in less than 10 msec, thus meeting the real-time operation requirement.

These modifications and others are intended to be encompassed by the following claims.

What is claimed is:

1.   A conoscopic topographer for obtaining topographic

2   measurements of a substantially spherical target surface at

3   a fixed position, comprising:

4   an illuminating device, producing a collimated

5   probe beam to said target surface, said probe beam being of

6   a probe wavelength to which said target surface is

7   reflective;

8   a collecting lens disposed relative to said target

9   surface at a predetermined distance, for receiving a

10   reflected probe beam including said target surface, said

11   reflected probe beam encoded with surface phase information

12   indicative of said target surface;

13   an optical birefringent medium having a single

14   optic axis, positioned relative to said collecting lens and

15   oriented to form a tilted angle between a direction of said

16   reflected probe beam and said optic axis, said birefringent

17   medium splitting said reflected probe beam into an ordinary

18   probe beam and an extraordinary probe beam which interfere

19   with each other to form a conoscopic interference pattern;

20   a first polarizer, located in an optical path of

21   said probe beam between said light source and said

22   birefringent medium, operating to polarize said reflected

23   probe beam in a first polarization direction;

24   an imager, receiving said conoscopic interference

25   pattern and producing an electrical representation of said

26   interference pattern; and

27   a microprocessor, processing said electrical

28   representation of said interference pattern to extract a

29   topographic shape of said target surface.

1   2.   A conoscopic topographer as in claim 1, wherein

2   said illuminating device has a partially coherent light

3   source.

1   3.   A conoscopic topographer as in claim 1, wherein

2   said illuminating device has an incoherent light source

3   which has a pin hole at an output thereof.

1   4.   A conoscopic topographer as in claim 1, wherein a

2   ratio of an spectral linewidth of said probe beam to said

3   probe wavelength is in a range from about 0.1% to about 1%.

1   5.   A conoscopic topographer as in claim 1, wherein

2   said collecting lens is so located relative to said target

3   surface that a spacing between two adjacent fringes in said

4   conoscopic interference pattern captured by said imager is

5   maximized.

1   6.   A conoscopic topographer as in claim 1, wherein

2   said first polarization is selected relative to said optic

3   axis of said birefringent medium so that said ordinary and

4   extraordinary beams have a substantially identical power

5   with respect to each other.

1   7.   A conoscopic topographer as in claim 1, wherein

-61-

2 said birefringent medium is a calcite crystal.

1   8.   A conoscopic topographer as in claim 1, wherein

2 said microprocessor extracts a direct phase information of

3 said target surface from said interference pattern by using

4 a Hermite polynomial expansion.

1   9.   A photorefractive keratectomy surgical system,

2 comprising:

3   a pulsed laser with a pulse repetition rate,

4 producing an ablating laser beam at a wavelength at which a

5 cornea is absorptive, said ablating laser beam having a

6 fluence sufficient to ablate cornea tissue;

7   a beam steering system, located relative to said

8 laser and guiding said ablating laser beam to a target eye

9 which is at a fixed location;

10   a conoscopic topographer disposed relative to said

11 fixed location, producing a probe beam to illuminate said

12 target eye and receiving a reflected probe beam from said

13   target eye, said topographer operable to measure a corneal

14   shape of said target eye based on a conoscopic interference

15   of said reflected probe beam; and

16   a system controller having a microprocessor,

17   electrically connected to said laser, said beam steering

18   system, and said topographer, said controller controlling

19   said topographer to achieve a corneal topographic

20   measurement of said target eye at a processing rate higher

21   than said pulse repetition rate.

1   10. A system as in claim 9, wherein said ablating

2   laser beam is controlled by said controller based on said

3   corneal topographic measurement of said target eye.

1   11. A system as in claim 10, wherein said control of

2   said ablating laser beam affects said fluence.

1   12. A system as in claim 10, wherein said control of

2   said ablating laser beam affects a beam impact position on

3   said target eye.

1   13. A system as in claim 9, wherein said topographer

2   comprises:

3   a light source, producing said probe beam;

4   a collimator, displaced relative to said light

5   source, operating to collimate said probe beam;

6   a collecting lens disposed relative to said target

7   eye at a predetermined distance for receiving said reflected

8   probe beam whose wavefront is encoded with corneal surface

9   phase information;

10   an optical birefringent crystal having a single

11   optic axis, positioned relative to said collecting lens and

12   orientated to form a tilted angle between a direction of

13   said reflected probe beam and said optic axis, said crystal

14   splitting said reflected probe beam into an ordinary probe

15   beam and an extraordinary probe beam which interfere with

16   each other to form a conoscopic interference pattern;

17   a first polarizer, located in an optical path of

18   said probe beam between said light source and said crystal,

19   operating to make said reflected probe beam polarize in a

20   first polarization direction;

21   an imager, receiving said conoscopic interference

22   pattern and producing an electrical representation of said

23   interference pattern; and

24   a second polarizer having a second polarization

25   direction substantially orthogonal to said first

26   polarization direction, located between said crystal and

27   said imager, said second polarizer optimizing a detection of

28   said imager.

1   14.   A method for performing a topographic measurement

2   of a spherical surface that is illuminated with a collimated

3   probe beam, comprising:

4   imprinting a phase information of said spherical

5   surface onto a reflected probe beam produced by said

6   illumination of said probe beam;

7   generating a conoscopic interference pattern by

8   using a uniaxial birefringent crystal to produce an ordinary

9   beam and an extraordinary beam from said reflected probe

10   beam;

11   determining a phase difference between said

12   ordinary and extraordinary beams;

13   detecting a two-dimensional positioning

14   representation of said spherical surface according to

15   positioning coordinates in said conoscopic interference

16   pattern;

17   extracting said phase information of said

18   spherical surface based on said phase difference; and

19   determining a three-dimensional representation of

20   said spherical surface.

1   15.   A method as in claim 14, wherein said phase

2   difference is determined by performing a phase shifting

3   process which comprises:

4   obtaining a first intensity distribution of said

5   conoscopic interference pattern at a first orientation of

6   said crystal to produce a first phase difference between

7   said ordinary and extraordinary beams;

8   obtaining a second intensity distribution of said

9   conoscopic interference pattern at a second orientation of

10   said crystal to produce a second phase difference between

11   said ordinary and extraordinary beams, said second

12   orientation being chosen so that said second phase

13   difference is shifted by about π/2 relative to said first

14   phase difference;

15   obtaining a third intensity distribution of said

16   conoscopic interference pattern at a third orientation of

17   said crystal to produce a third phase difference between

18   said ordinary and extraordinary beams, said third

19   orientation being chosen so that said third phase difference

20   is shifted by about π relative to said first phase

21   difference; and

22   obtaining a fourth intensity distribution of said

23   conoscopic interference pattern at a fourth orientation of

24   said crystal to produce a fourth phase difference between

-67-

25   said ordinary and extraordinary beams, said fourth

26   orientation being chosen so that said fourth phase

27   difference is shifted by about 3π/2 relative to said first

28   phase difference.

1   16. A method as in claim 14, wherein said extracting

2   of said phase information from said phase difference

3   comprises:

4   representing said phase difference by a first

5   polynomial expansion of Hermite polynomials to a first

6   number of terms;

7   representing said phase difference by a second

8   polynomial expansion of Hermite polynomials to a second

9   number of terms, said second number bing smaller than said

10   first number by one;

11   determining a second set of expansion coefficients

12   of said second polynomial expansion by projecting said phase

13   difference in a vector space formed by said Hermite

14   polynomials; and

-68-

15   determining a first set of expansion coefficients

16   of said first polynomial expansion based on said second set
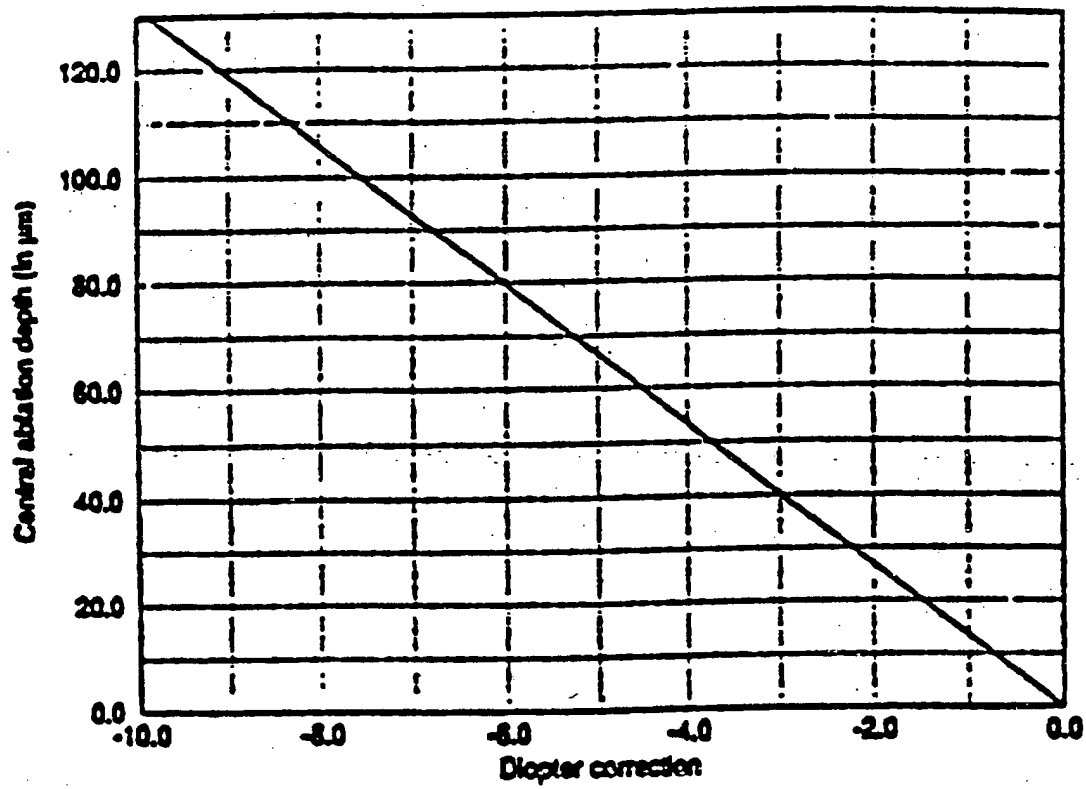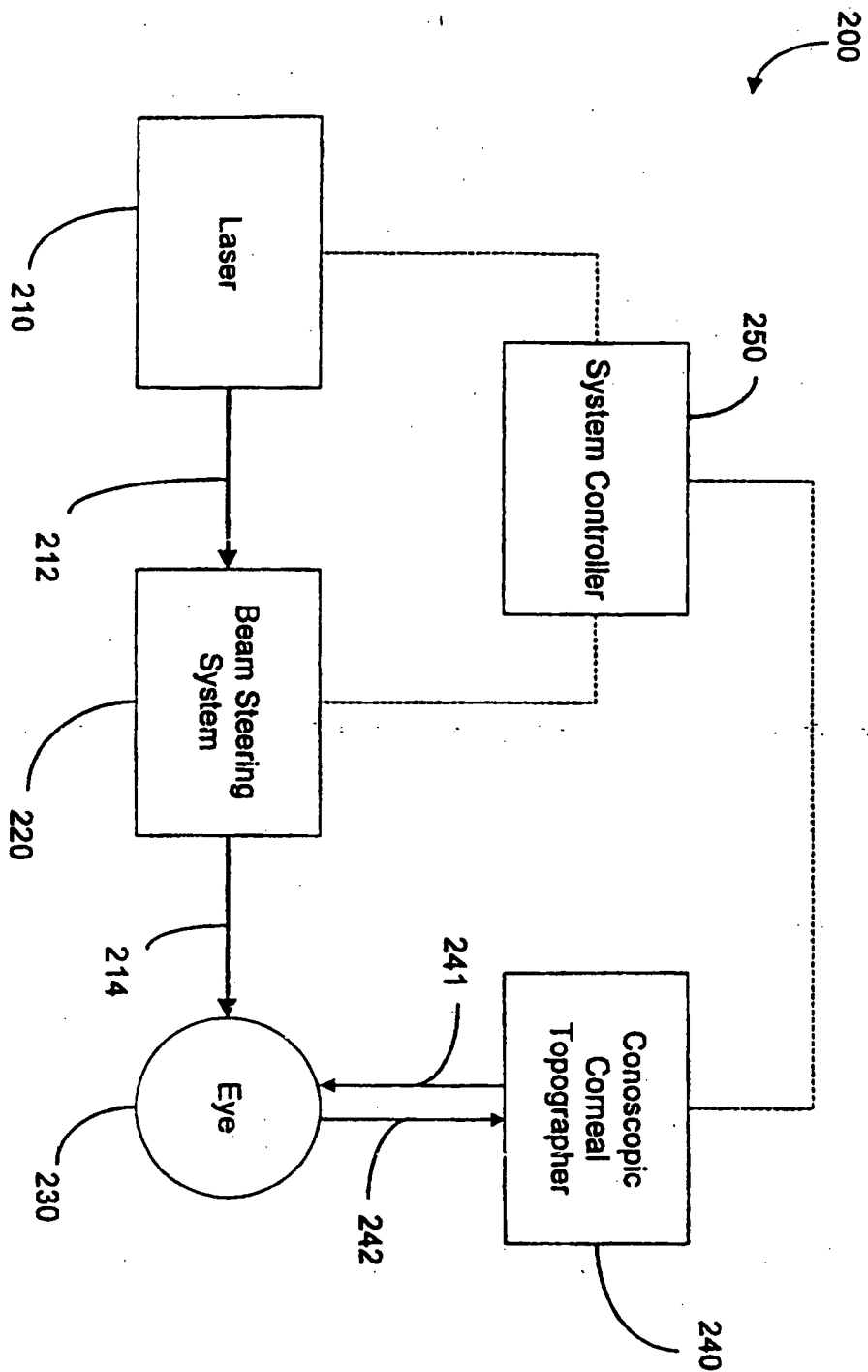
17   of expansion coefficients.

FIG 1
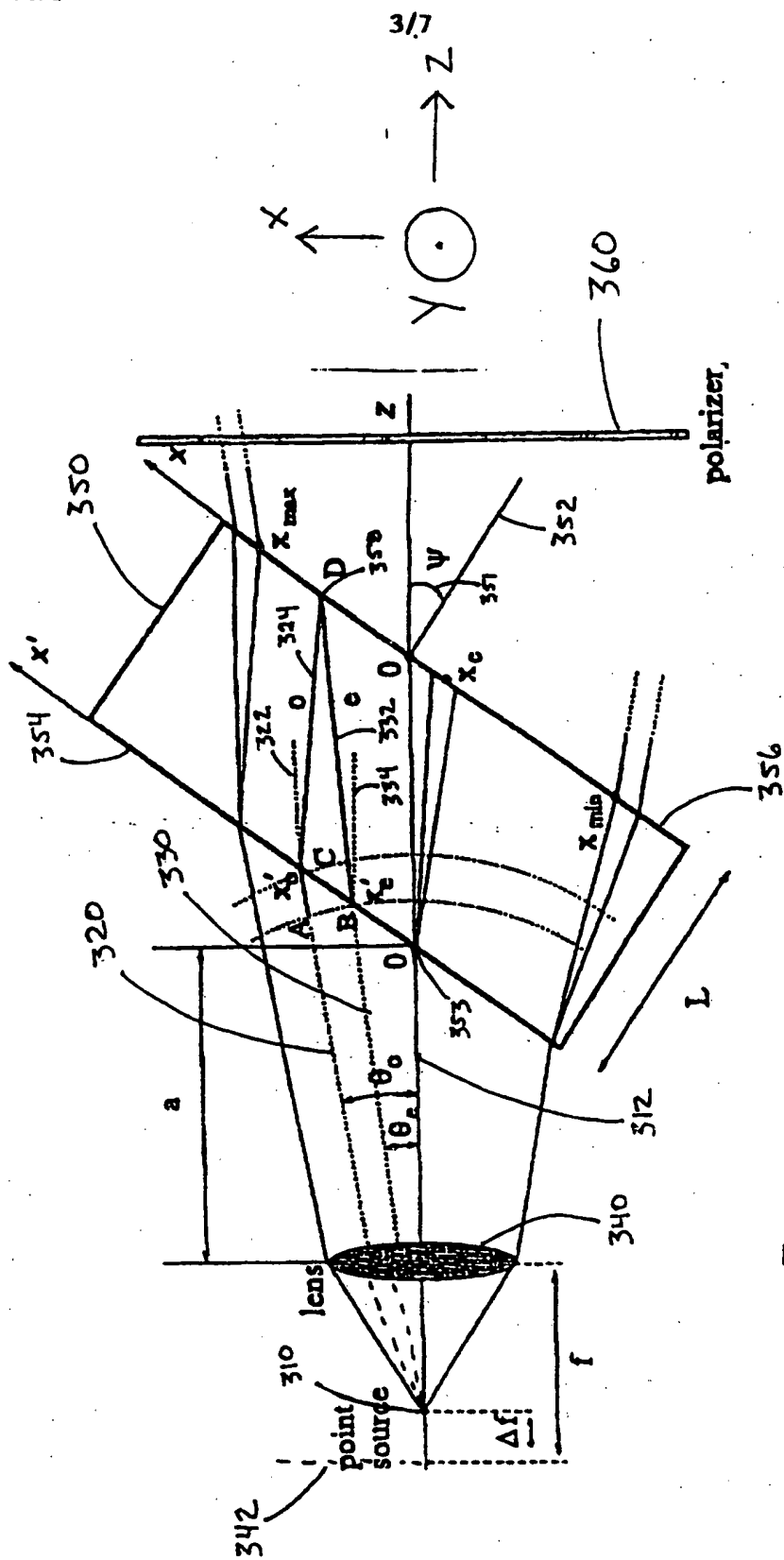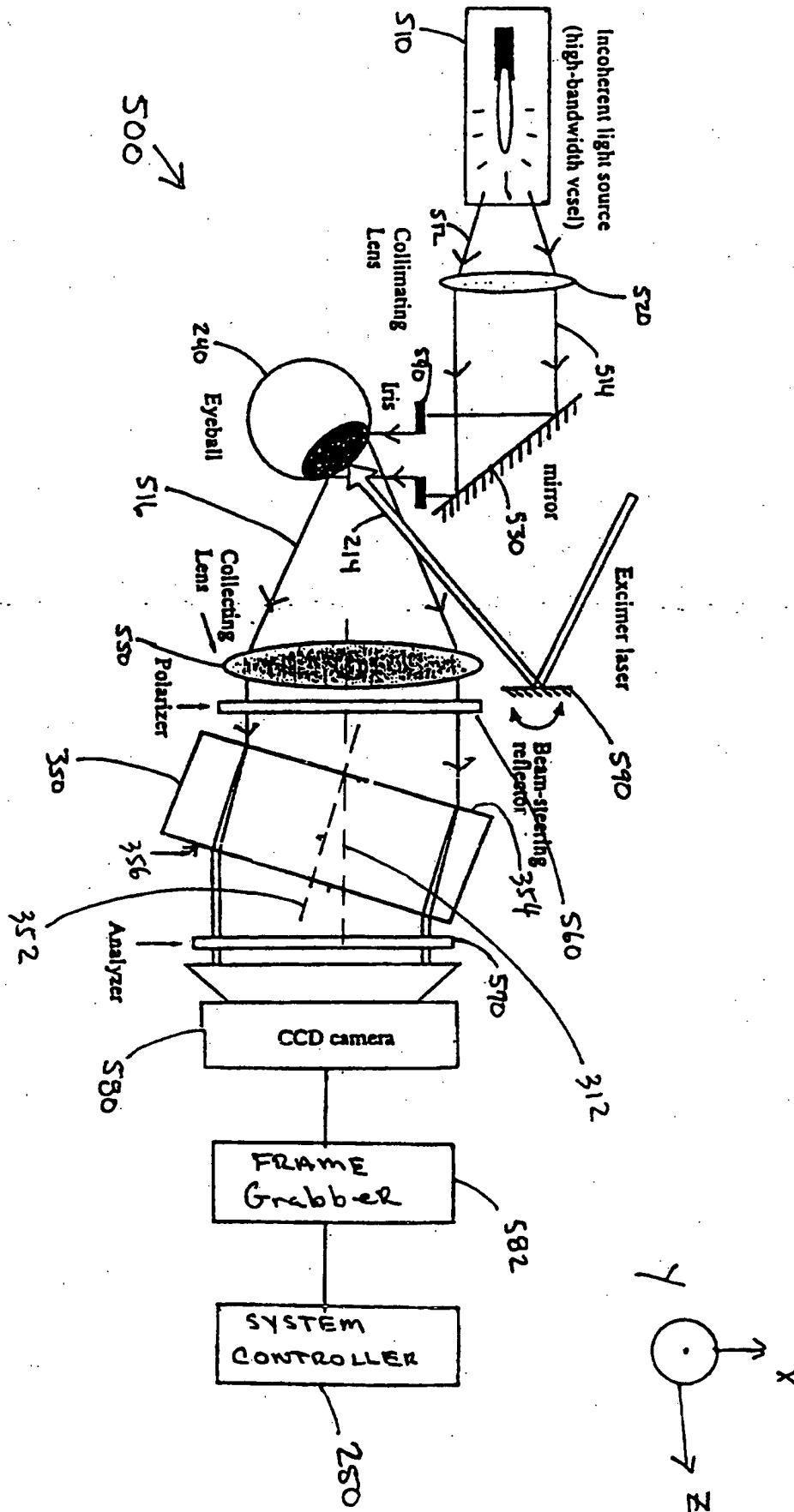
FIG. 2
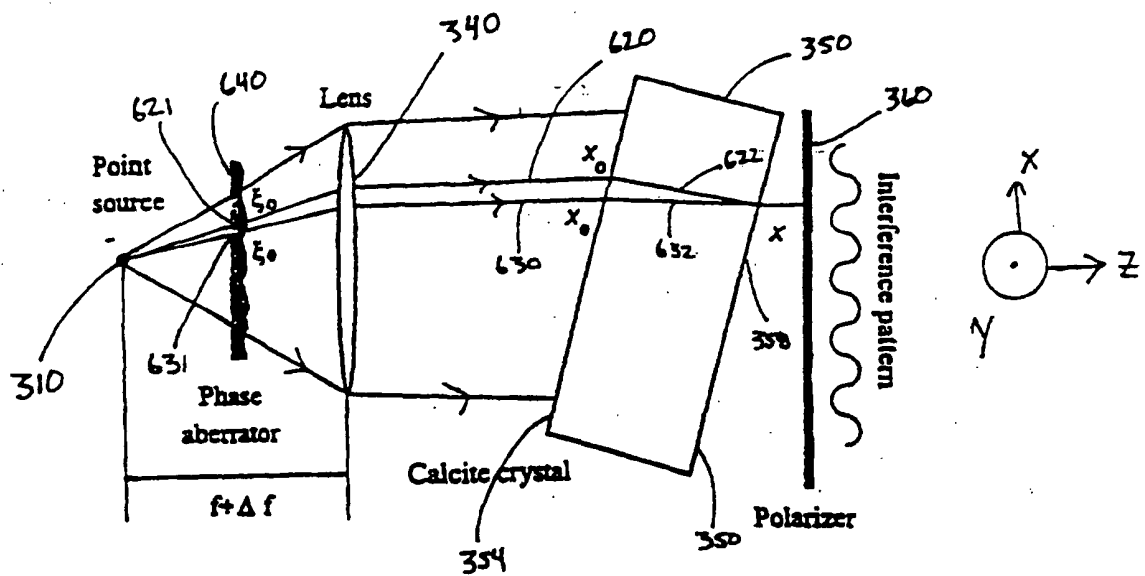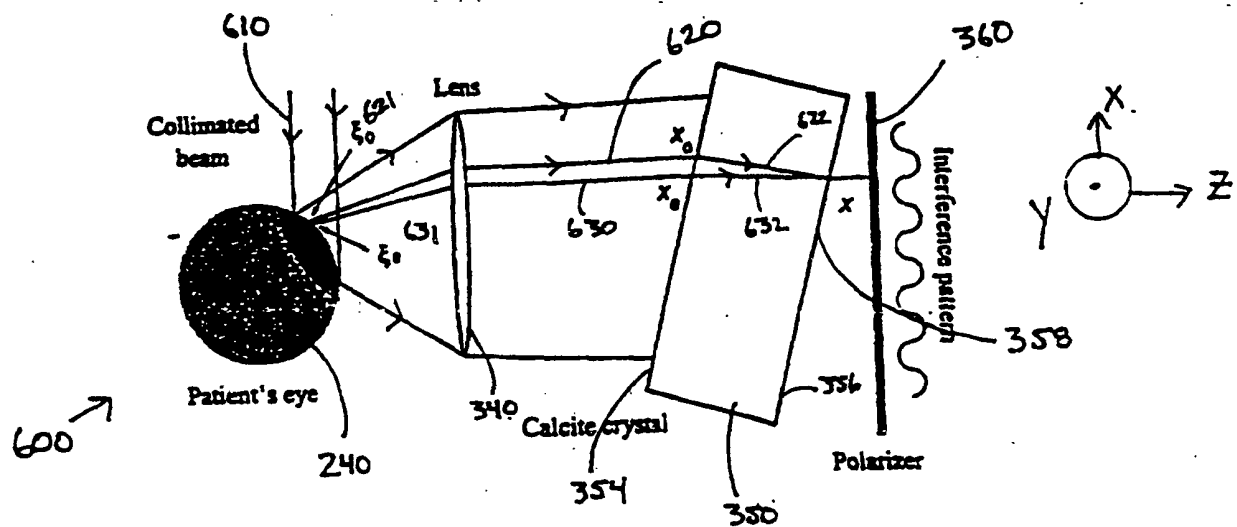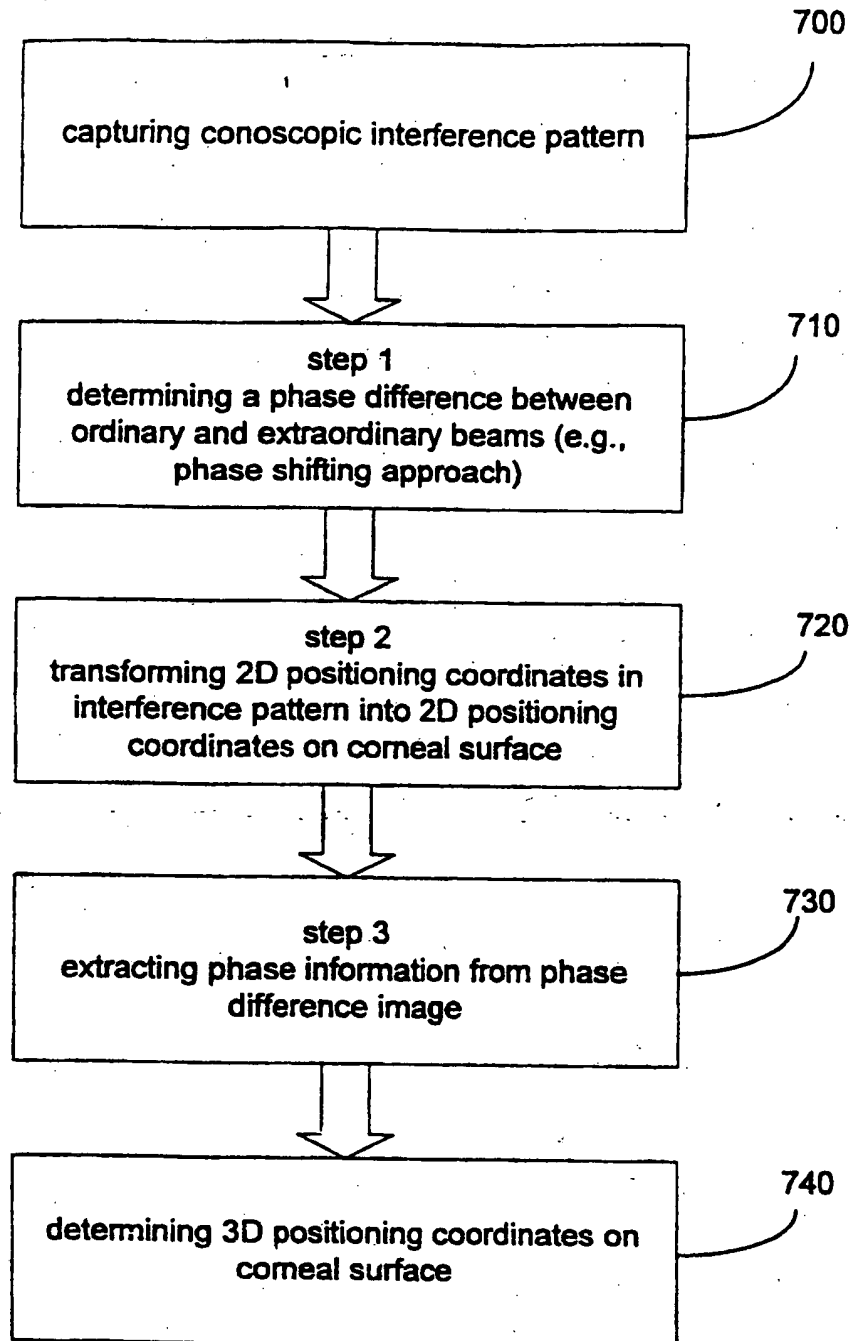
200

Laser 210

System Controller 250

212

Beam Steering System 220

214

Eye 230

241

242

Conoscopic Corneal Topographer 240

FIG. 3

FIG 4

FIG. 5

500

Incoherent light source (high-bandwidth vcsel) 510

512

Collimating Lens 520

514

Iris 540

540 Eyeball

mirror 530

Collecting Lens 516

214

Excimer laser

Beam-steering reflector 590 560

Polarizer 550

350

356

352

Analyzer

354

570

312

CCD camera 580

FRAME Grabber 582

SYSTEM CONTROLLER 250

Y

X

Z

FIG 6B

FIG 6A

FIG. 7

INTERNATIONAL SEARCH REPORT

A.   CLASSIFICATION OF SUBJECT MATTER

IPC(6)   :A61B 17/36; G01B 9/021
US CL   :356/347; 606/5
According to International Patent Classification (IPC) or to both national classification and IPC

B.   FIELDS SEARCHED

Minimum documentation searched (classification system followed by classification symbols)

   U.S. :   351/211, 212, 216, 246; 356/124, 345, 347, 365; 606/2-6

Documentation searched other than minimum documentation to the extent that such documents are included in the fields searched

Electronic data base consulted during the international search (name of data base and, where practicable, search terms used)

C.   DOCUMENTS CONSIDERED TO BE RELEVANT

Category*	Citation of document, with indication, where appropriate, of the relevant passages	Relevant to claim N .
A,P	US 5,549,599 A (SUMIYA) 27 August 1996, entire document.	1, 9, 14
A,P	US 5,613,965 A (MÜLLER) 25 March 1997, entire document.	1, 9, 14
A	US 5,395,356 A (KING et al) 07 March 1995, entire document.	1, 9, 14

☐   Further documents are listed in the continuation of Box C.   ☐   See patent family annex.

*	Special categories of cited documents:	"T"	later document published after the international filing date or priority date and not in conflict with the application but cited to understand the principle or theory underlying the invention
"A"	document defining the general state of the art which is not considered to be of particular relevance		
"E"	earlier document published on or after the international filing date	"X"	document of particular relevance; the claimed invention cannot be considered novel or cannot be considered to involve an inventive step when the document is taken alone
"L"	document which may throw doubts on priority claim(s) or which is cited to establish the publication date of another citation or other special reason (as specified)		
		"Y"	document of particular relevance; the claimed invention cannot be considered to involve an inventive step when the document is combined with one or more other such documents, such combination being obvious to a person skilled in the art
"O"	document referring to an oral disclosure, use, exhibition or other means		
"P"	document published prior to the international filing date but later than the priority date claimed	"&"	document member of the same patent family

Date of the actual completion of the international search	Date of mailing of the international search report
31 JULY 1997	2 7 AUG 1997
Name and mailing address of the ISA/US Commissioner of Patents and Trademarks Box PCT Washington, D.C. 20231	Authorized officer BRYAN YARNELL